Radiation Physics and Chemistry 220 (2024) 111709

Contents lists available at ScienceDirect

Radiation Physics and Chemistry

journal homepage: www.elsevier.com/locate/radphyschem

Debye-Waller effects in Bethe-Salpeter calculations: Bridging the gap between XANES and EXAFS

Eric L. Shirley [a,*], Joseph C. Woicik [b]

[a] Sensor Science Division, Physical Measurement Laboratory, NIST, Gaithersburg, MD, 20899, USA
[b] Materials Measurement Science Division, Material Measurement Laboratory, NIST, Gaithersburg, MD, 20899, USA

ARTICLE INFO

Handling Editor: Chris Chantler

Keywords:
Bethe-Salpeter equation
Debye-Waller
Theory
X-ray absorption

ABSTRACT

We present a method to incorporate Debye-Waller effects on core-excitation spectra within frameworks other than real-space, multiple-scattering formulations. The method draws ideas used in multiple-scattering theory to realize effects of variations in interatomic distances, and the method accomplishes this without benefit of the atom-by-atom nature in which multiple-scattering calculations are formulated. We test the method in four metals and one semiconductor over a range of temperatures and compare all theoretical results to experiment. The method is agnostic regarding the source of interatomic distance information, and it should be applicable to a wide range of systems, including systems without crystalline periodicity.

1. Introduction

This work considers x-ray absorption near-edge spectroscopy (XANES) calculations, which typically treat, say up to the first ~ 100 eV above an x-ray edge. Conversely, most practical extended x-ray absorption fine-structure spectroscopy (EXAFS) analysis emphasizes higher energy regions. It is for practical reasons that *two* complementary theoretical approaches (XANES and EXAFS) are used in this way. XANES analysis typically focuses on electronic states in a core-excited system and is exemplified by Bethe-Salpeter equation [Shirley et al., 2020, Gilmore et al., 2015] and excited core-hole (XCH) [Taillefumier et al., 2002,Prendergast and Galli, 2006] approaches that work best and are easiest to apply close to an edge. EXAFS analysis relies on real-space multiple-scattering theory that works best and is easiest to apply far above an edge.

Inclusion of Debye-Waller (DW) effects has been a longstanding essential part of EXAFS analysis. There exist several reviews of basic EXAFS theory, including ones that treat DW effects [Stern, 1974, Ashley and Doniach, 1975, Lee and Pendry, 1975, Lee et al., 1981, Rehr and Albers, 2000]. EXAFS analysis usually interprets spectral features within a picture featuring a photoelectron excited from an absorbing atom's core. The electron has wave vector k (which depends on photon energy E) and scattering multiple times from the atoms in the system. The simplest scattering process involves the electron backscattering from an atom near the core-excited site before re-scattering from the core-excited site. EXAFS oscillations (or the "EXAFS signal") result from interference between the original outgoing and the re-scattered waves that travel distances differing by the closed-loop path length that was traveled upon returning to the core-excited site. For each backscatterer, oscillations are roughly a periodic function of k. Debye-Waller (DW) effects result from fluctuations in interatomic distances weakening EXAFS oscillations by a gaussian function of k. Higher-order moments of variations in interatomic distances can be treated using cumulant approaches.

There is scant comparable inclusion of DW effects in theoretical near-edge work. Recent studies including effects of atomic displacements are the work of Vinson et al. [Vinson et al., 2016], Pascal et al. [Pascal et al., 2014], Brouder et al. [Brouder et al., 2010], and Cockayne et al. [Cockayne et al., 2018]. Strictly speaking, the above-mentioned complementarity is only one of theoretical approaches (XANES and EXAFS), not of spectral regions treated. Neglect of DW effects in XANES calculations hampers comparison with EXAFS calculations. In what follows, we summarize elementary aspects of EXAFS theory to elucidate how DW effects are treated. This suggests how one can model DW effects in a XANES calculation, and we described a scheme for that purpose. We then model DW effects within XANES calculations in the metals, copper, aluminum, and lead, and the semiconductor, germanium. These materials were selected for reasons of availability of data and/or interesting aspects related to the DW effects, such as the low melting temperature of lead and insight about the unoccupied density of states in germanium.

* Corresponding author.
E-mail addresses: eric.shirley@nist.gov (E.L. Shirley), woicik@bnl.gov (J.C. Woicik).

https://doi.org/10.1016/j.radphyschem.2024.111709
Received 24 November 2023; Received in revised form 13 March 2024; Accepted 20 March 2024
Available online 22 March 2024
0969-806X/Published by Elsevier Ltd.

All of our results are presented over a range of temperatures and compared to experimental results.

2. DW effects in EXAFS theory

There is a "step up" or "edge jump" in the absorption spectrum of a material wherever E exceeds a core-level binding energy. Above that transition the absorption coefficient, $\mu(E) = \mu_0(E) + \Delta\mu(E)$, has contributions from all shallower shells, $\mu_0(E)$, and from the shell of interest, $\Delta\mu(E)$. One can isolate these from each other, because $\mu_0(E)$ can be extrapolated from below an edge to above. The "EXAFS signal" is $\chi(k) = [\Delta\mu(E) - \mu_0(E)]/\Delta\mu_0(E)$, where $\Delta\mu_0(E)$ is whatever $\mu(E) - \mu_0(E)$ would be without backscattering. A mainstay equation in EXAFS theory is the "EXAFS equation,"

$$\chi(k) = S_0^2 \sum_j \frac{|f_j(k)|}{kR_j^2} \sin\left[2kR_j + 2\delta_c + \Phi_j(k)\right] e^{-2R_j/\lambda(k)} e^{-2\sigma_j^2 k^2} + \ldots \quad (1)$$

Terms not shown would account for closed-loop paths with more than two segments. The prefactor S_0^2 is an overall factor accounting for many-body effects not discussed here [Rehr and Albers, 2000]. The index j sums over atoms surrounding the core-excited site, $f_j(k)$ and $\Phi_j(k)$ are the complex scattering amplitude and associated phase shift for each atom, δ_c is the central scattering phase shift, and the first exponential includes photoelectron and core-hole self-energy damping. The gaussians in Eq. (1) arises from DW effects and follows from convolution of the sine function in Eq. (1) with a gaussian distribution of the closed-loop path length to atom j and back, with σ_j being the standard deviation of the interatomic distance.

3. Incorporating debye-waller effects in XANES spectra

The Fourier transform of $\chi(k)$ with respect to k has peaks near places expected from interatomic distances. The peaks are not arbitrarily sharp, and their heights are finite, because of self-energy damping, DW effects, and the decrease of $|f_j(k)|$ at large k. Furthermore, energy-dependence of the scattering phase shifts displaces the peaks' centroids from expected locations. If the gaussians in Eq. (1) were initially omitted, as is the case in a "raw" theoretical XANES spectrum, the following three steps would be an equivalent way to include them: (1.) Fourier transformation of $\chi(k)$ to a real-space domain, (2.) windowed convolutions of portions of the transform with gaussians reflecting fluctuations of interatomic distances, and (3.) Fourier transformation back to the k domain.

We will now apply the last insight to XANES analysis. This is justified, in part, because the methodology must work well at the high-k end of the XANES region. However, it might also work sufficiently well closer to an edge, where DW effects grow small at small k and so cannot be poorly modeled in an absolute sense. They should not vanish altogether, however, because the value of k at an edge is not zero but better estimated from the occupied width of whatever nearly-free-electron band structure begins below and continues into the unoccupied bands. This latter point has been made, for instance, by Rehr and Albers [Rehr and Albers, 2000] and Stern et al. [Stern et al., 1991]. It is still helpful, then, to consider the XANES signal as the Fourier transform of a closed-loop path-length distribution function (PLDF) weighted by core photoexcitation matrix elements. To define what is meant by "DW effects" on spectral features within a XANES calculation, we denote a raw XANES spectrum (without DW effects) $S_0(k)$ and the corresponding, affected spectrum (with DW effects) $S_1(k)$.

The unaffected PLDF is

$$a(l) = \int \frac{dk}{2\pi} e^{ikl} S_0(k). \quad (2)$$

This will not have sharp peaks as in the EXAFS case, because a XANES calculation k range is usually small. Nonetheless, use of the alternative three steps serves as an artifice to incorporate the salient DW effects. The affected PLDF is found by convolution with gaussians whose width depend on the path length:

$$b(l) = \int dl'\, g(l - l', |l'|) a(l'). \quad (3)$$

The gaussian, is

$$g(l - l', |l'|) = \left(\frac{1}{8\pi\sigma^2(|l'|)}\right)^{1/2} \exp\left(-\frac{(l - l')^2}{8\sigma^2(|l'|)}\right). \quad (4)$$

Its normalization ensures that spectral weight is conserved, and the standard deviation is $2\sigma(|l'|)$. In EXAFS $\sigma(l')$ is the standard deviation of an interatomic distance, but here the values of l' form a continuum. We assume $\sigma(|l'|)$ is known, because it can be found by a variety of methods, of which we mention a few later. One has $\sigma(0) = 0$, with $\sigma(|l'|)$ increasing approximately linearly with path length until it fluctuates around a value that we denote σ_∞. In this way, $\sigma(|l'|)$ mimics the average fluctuations for atoms beyond some distance as well as those for the first few coordination shells. With minor approximation, we shall assume $\sigma(|l'|) = \sigma_\infty$ for $|l'| > l_c$ (typically around the third coordination shell, but more detail can be included).

The affected spectrum is

$$S_1(k) = \int dl\, e^{-ikl} b(l). \quad (5)$$

Having

$$g(l_1 - l_0, |l_0|) = g(l_1 - l_0, \infty) + \left[g\left(l_1 - l_0, |l_0|\right) - g(l_1 - l_0, \infty)\right] \quad (6)$$

implies

$$\frac{\delta S_1(k_1)}{\delta S_0(k_0)} = t_\infty(k_1, k_0) + t_r(k_1, k_0), \quad (7)$$

with

$$t_\infty(k_1, k_0) = e^{-2\sigma_\infty^2 k_0^2} \delta(k_1 - k_0) \quad (8)$$

and

$$t_r(k_1, k_0) = \frac{1}{2\pi} \int_{-l_c}^{+l_c} dl_0\, e^{i(k_0 - k_1)l_0} \left[e^{-2\sigma^2(l_0)k_1^2} - e^{-2\sigma_\infty^2 k_1^2}\right]. \quad (9)$$

Thus, an EXAFS feature is preserved in $S_1(k_1)$ but with reduced strength via $t_\infty(k_1, k_0)$, whereas its remainder "dissolves" into a Gaussian-like distribution surrounding k_0 via $t_r(k_1, k_0)$. [Photoelectron- and core-level lifetime-damping broaden the delta function in Eq. (8).] The before-and-after overall oscillator strengths are related to $a(0)$ and $b(0)$, and they barely differ because one usually has $\sigma(l) \ll l$. [To be precise, electron states that give rise to spectral features are not broadened in energy by DW effects, but the features are modified by DW effects on the on-site photoelectron partial-wave amplitude (for the initial and subsequently scattered partial waves) that depends on energy (or k). This arises, it appears, through a change in electron states' wave functions. Hence, any "local density of states" actually fluctuates all the time because of fluctuations in atomic coordinates and their effects on local values of wave functions.]

We obtained values of $\sigma(|l'|)$ for $|l'| < l_c$ at $n + 1$ values of $|\,l'\,|$ denoted by l_m with $0 \le m \le n$. Adjacent values of l_m differed by about 25 pm or less. One has $l_0 = 0$ and $l_n = l_c$. We used the Beni-Platzman formula [Beni and Platzman, 1976] for $\sigma(|l'|)$ in metals, whereas for germanium we interpolated between the values of $\sigma(|l'|)$ for the first three coordinate shells obtained along with those reported by Woicik et al. [Woicik et al., 2023]. Given $\sigma(l_m)$ and $\sigma(l_{m+1})$, we interpolated the gaussian according to

$$g(\lambda, l_m < |\acute{l}| < l_{m+1}) \approx \left(\frac{l_{m+1}-|\acute{l}|}{l_{m+1}-l_m}\right) g(\lambda, l_m) + \left(\frac{|\acute{l}|-l_m}{l_{m+1}-l_m}\right) g(\lambda, l_{m+1}) \ . \quad (10)$$

This implied the approximation,

$$b(l) \approx \sum_{m=0}^{n} \int d\acute{l}\ w_m(\acute{l}) g(l-\acute{l}, l_m) a(\acute{l}), \quad (11)$$

and use of only $2n+1$ convolutions, with $w_m(\acute{l})$ determined by Eq. (10) and $\sigma(|\acute{l}| > l_\infty) = \sigma_\infty$.

Besides EXAFS oscillations, a near-edge spectrum also includes *bona fide* near- and/or pre-edge core-hole multiplet and/or densities-of-states structure and a roughly energy-independent part whose height is the edge jump. These should be less susceptible to DW effects but be influenced by Franck-Condon effects and *E-e* Jahn-Teller instabilities [Bersuker and Polinger, 1989,de Groot et al., 1990,Tinte and Shirley, 2008, Gilmore and Shirley, 2010]. More generally, it is also advisable to consider core hole-exciton features differently. On the other hand, an edge jump reflects the onset of unoccupied portions of valence bands in metals and/or conduction bands in insulating systems, whereas there may be no jump in the density of states (DOS), which is a single, continuous function referred to as the "occupied DOS" below the Fermi level and "unoccupied DOS" above the Fermi level. In practice these details are readily captured in band-structure-based calculations (e.g., BSE) but not in multiple-scattering frameworks owing to the large number of scattering paths.

The edge jump can be spuriously affected in the present method, however, unless mitigating steps are taken. Formally, a step function has a non-zero Fourier transform for all l, although it has nothing to do with path lengths. Any associated artifacts are expected to be small, because DW effects are small at the edge, where $\hbar^2 k_0^2/(2m_e)$ (the kinetic energy of a notional nearly-free photoelectron at the edge jump) is roughly only the nominal valence bandwidth (about 10 eV in Cu, 12 eV in Ge, 11 eV in Al, and 12 eV in Pb). If $\Theta_0(k)$ is the spectrum resulting from lifetime broadening of a spectrum given by $\theta(k-k_0)$ that omits DW effects, and $\Theta_1(k)$ differs only because it includes DW effects, artifacts are improved by the replacement,

$$S_1(k) \rightarrow S_1(k)\Theta_0(k) \ / \ \Theta_1(k) \quad (12)$$

and completely removed for a step function. In addition, there is no need to normalize the step function considered for such a *multiplicative* correction, and the ratio $\Theta_0(k)/\Theta_1(k)$ is smooth except near the edge jump, so real spectral features are largely immune to application of Eq. (12).

Core hole-lifetime and energy-resolution broadening can be applied after including DW effects, so one can also manually remove any spurious spectral weight below the edge prior to such broadening. [In this work, though, it was convenient to include photoelectron-lifetime broadening (which is zero at the edge) before applying DW effects.] One can also alternately include or omit the step indicated in Eq. (12), which allows one to estimate the much smaller effects of any residual artifacts, including ambiguity regarding energy placement of the step-function discontinuity. In metals, one can likewise apply DW effects to the entire, core-hole-perturbed, matrix-element-weighted DOS before applying a Fermi factor to account for the Pauli exclusion principle and remaining broadening.

4. Demonstration applications

We now consider inclusion of DW effects in XANES spectra for metallic copper (Cu), aluminum (Al), and lead (Pb), as well as the semiconductor, germanium (Ge). The underlying methodology for the XANES calculations was presented by Shirley and Woicik [Shirley and Woicik, 2022]. For the Beni-Platzman treatment of $\sigma(\acute{l})$, it is necessary to know the Debye temperature for the metals, which we assumed to be 343 K, 394 K, and 88 K for Cu, Al and Pb, respectively. In all of what is presented, the energy of the theoretical edge was adjusted to align with experiment, as is commonly done in practice. Regarding the vertical scales of spectra, each spectrum was normalized to have a consistent baseline and edge jump in Figs. 1, 2 and 5. However, In Figs. 3 and 4, scaling of features were chosen to be consistent according to the originally produced experimental results. (The same scaling was applied to everything calculated or to everything measured.)

Fig. 1 shows a measured Cu 1s near-edge spectrum and theoretical spectra omitting DW effects and including DW effects for 10 K and 300 K. At higher energies, EXAFS oscillations are grossly overestimated without including DW effects, and even zero-point-motion is appreciable. (For all materials, close examination of spectral features at the edge also suggests other improvements outside the scope of this work.) A similar comparison is made in Fig. 2 for the Al 1s near-edge spectrum, comparing our results and the XANES results provided by Balerna [Balerna, 2019]. Fig. 3 emphasizes a portion of our theoretical absorption spectrum and the EXAFS signal reported in the same work by Balerna. These are given as a function of k and cannot be directly compared, but the similarity of temperature dependences is encouraging.

Lead has a relatively low melting point (about 600 K), and Stern et al. [Stern et al., 1991] analyzed EXAFS below, near and above the melting transition. Fig. 4 shows the near-edge spectrum starting near the top of the edge jump for low, ambient, and near-melting temperatures. The energy scale is relative to the edge, and the vertical scale is in units of the edge jump. While similarity of features and their temperature dependence is gratifying, agreement between our result and measurements so near a melting point might be partly fortuitous.

Fig. 5 shows measured and calculated Ge 1s spectra at 8 K and 375 K. In the difference spectra shown, cancellation of smooth features distills and clarifies finer features suppressed by DW effects at 375 K. [There is also a small (about 0.1 eV) energy shift of the edge jump with temperature that was measured and incorporated into the calculated spectra.] The finer features are also difficult to resolve in native germanium because of the large Ge 1s level width [Campbell and Papp, 2001], but the underlying DOS features have been elucidated for Ge using the Si 1s edge of a dilute Si-in-Ge alloy [Woicik et al., 1988, Woicik and Pianetta,

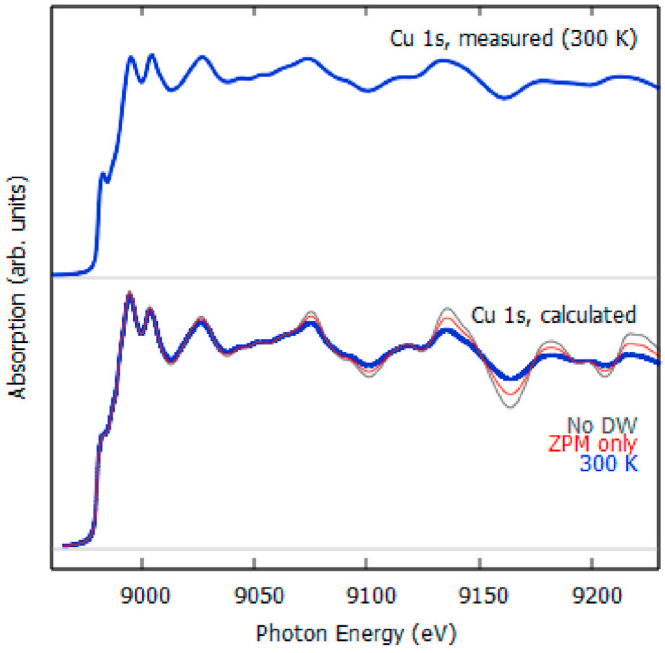

Fig. 1. The authors' measured Cu 1s 300 K npeear-edge spectrum (top) and calculated spectra (bottom) that omit DW effects (grey), only include zero-point motion (ZPM) (red), and include 300 K DW effects (blue). (So the ZPM result is equivalent to 0 K.) Spectra are offset for clarity.

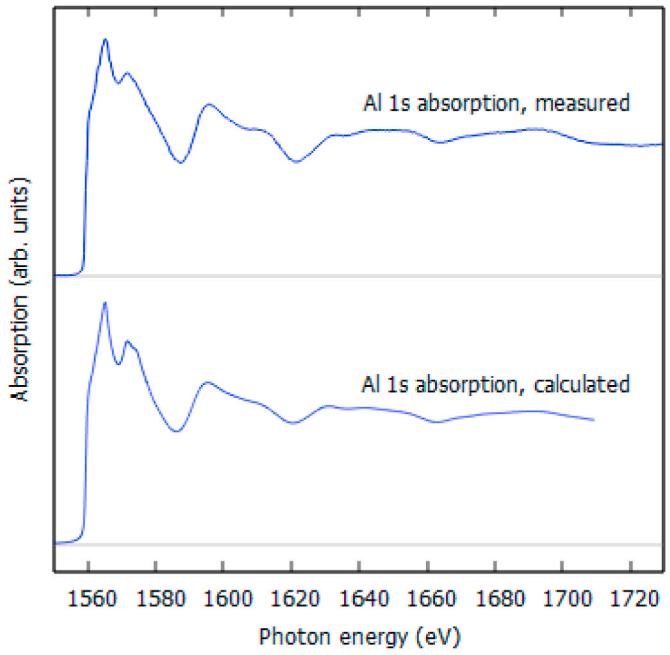

Fig. 2. Al 1s room-temperature near-edge spectrum as measured [Balerna, 2019] (top) and calculated (bottom). Spectra are offset for clarity.

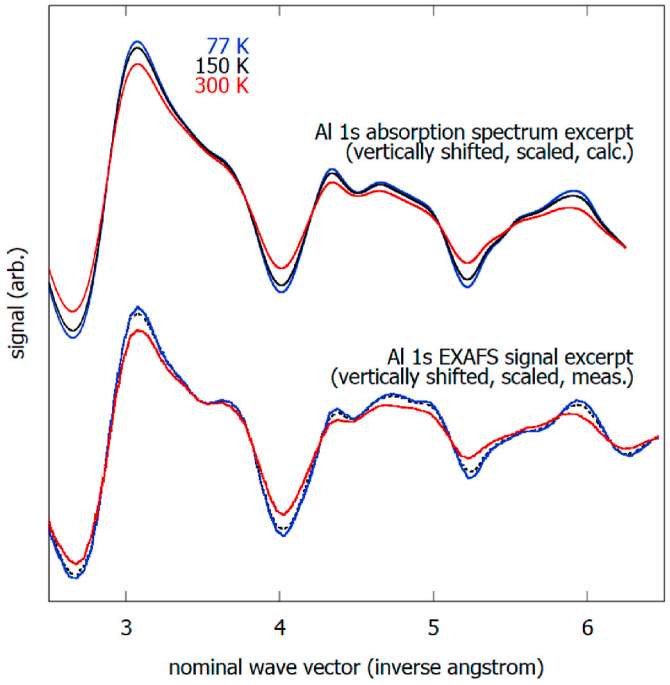

Fig. 3. An isolated portion of the Al 1s absorption spectrum at 3 temperatures (top, theory) and a corresponding portion of the XAFS signal (bottom, experiment) taken from Balerna [Balerna, 2019]. Spectra are offset for clarity.

1992] that was also simulated by the authors [Shirley and Woicik, 2022]. The overall qualitative agreement is nonetheless clear. Regarding remaining discrepancies between calculated and measured difference spectra, we note that genuine measured features were confirmed by the alloy spectrum, and genuine calculated features were confirmed when examining spectra with artificially narrow lifetime broadening applied. It is also true (see [Woicik et al., 2023]) that calculated spectra can underestimate some structure far above the edge for two reasons. One reason is approximations in the wave functions of calculated electron

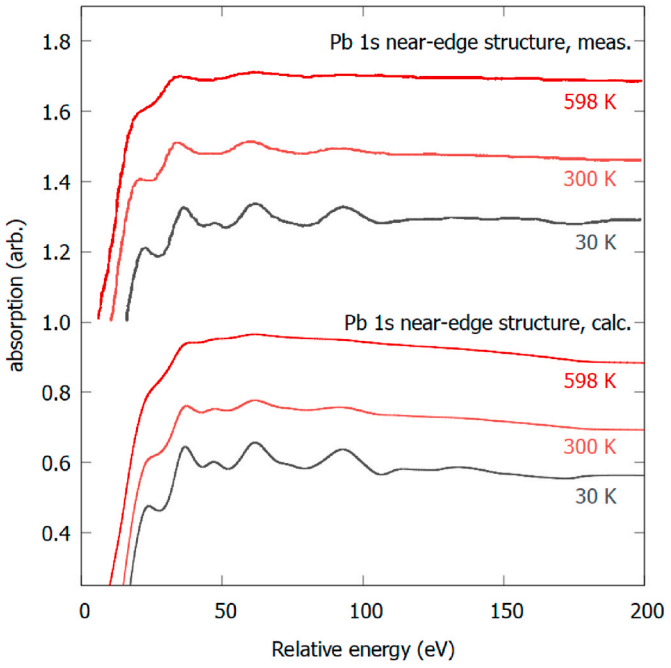

Fig. 4. Pb 1s near-edge structure. For each temperature (indicated by color), with energy relative the edge jump as given by Stern et al. [Stern et al., 1991]. Spectra are offset vertically for clarity. Measured spectra are shown at top, and calculated spectra are shown at bottom.

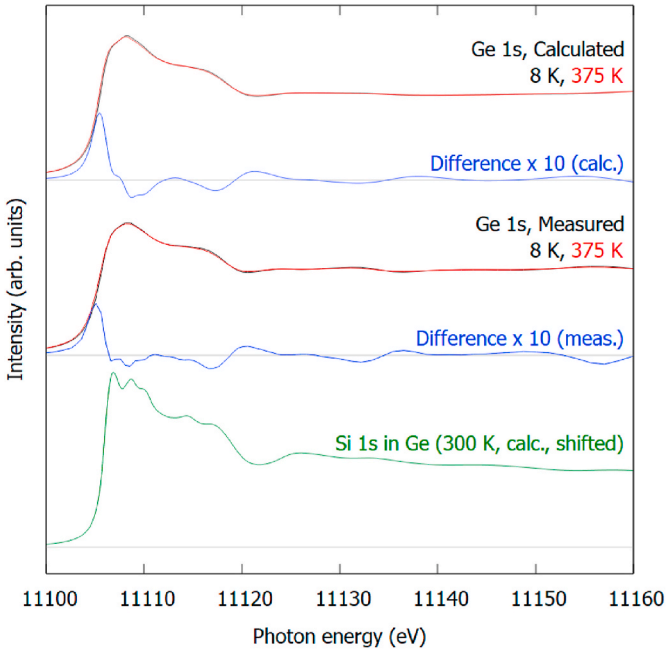

Fig. 5. The authors' Ge 1s near-edge spectra for low (8 K) and high (375 K) temperatures and difference spectra as measured (top) and calculated (middle). A theoretical, energy-shifted Si 1s near-edge spectrum is also shown for a dilute Si-in-Ge alloy, bolstering confidence regarding fine structure elicited in difference spectra. Spectra are offset for clarity.

states. The other reason is overestimation of lifetime damping far above an edge.

5. Conclusions

We have presented a method to include Debye-Waller effects within

a framework suitable for x-ray absorption near-edge spectroscopy calculations. The method requires a theoretical spectrum that omits such effects (preferably before lifetime broadening is applied) and knowledge about fluctuations of interatomic distances. To the extent that "single-scattering" processes dominate extended x-ray absorption fine structure effects, the method should have great efficacy. However, even when the "single-scattering" approximation breaks down, the method should include Debye-Waller effects reasonably well. We demonstrate this with examples in several crystalline systems, but the method should also work in other systems. In addition to calculations that rely on solution of the Bethe-Salpeter equation, the method should be equally useful in related (allied) calculations such as those using the random-phase approximation and/or time-dependent density-functional theory, as well as calculations that omit electron-core hole interactions altogether. One of our intentions is that computed XANES and EXAFS spectra can be calculated well enough so that there is an energy overlap region with agreeing results instead of having an energy separation (gap) or threshold between regions where each method is suitable. The authors thank Antonella Balerna for sharing a measured aluminum 1s spectrum and for fruitful discussions. The authors also benefited from discussions with John J. Rehr.

CRediT authorship contribution statement

Eric L. Shirley, Joseph C. Woicik: Conceptualization, Data curation, Formal analysis, Methodology, Writing – original draft, Writing – review & editing.

Declaration of competing interest

The authors declare that they have no known competing financial interests or personal relationships that could have appeared to influence the work reported in this paper.

Data availability

Data will be made available on request.

References

Ashley, C.A., Doniach, S., 1975. Theory of extended x-ray absorption edge fine structure (EXAFS) in crystalline solids. Phys. Rev. B 11, 1279.
Balerna, A., 2019. DAFNE-light DXR1 soft X-ray synchrotron radiation beamline: characteristics and XAFS applications. Condens. Matter 4, 7.
Beni, G., Platzman, P.M., 1976. Temperature and polarization dependence of extended x-ray absorption fine-structure spectra. Phys. Rev. B 14, 1514.
Bersuker, I.B., Polinger, V.Z., 1989. Vibronic Interactions in Molecules and Crystals. Springer, Berlin.
Brouder, C., Cabaret, D., Juhin, A., Sainctavit, P., 2010. Effect of atomic vibrations on the x-ray absorption spectra at the K edge of Al in α-Al_2O_3 and of Ti in TiO_2 rutile. Phys. Rev. B 81, 115125.
Campbell, J.L., Papp, T., 2001. Widths of the atomic K-N7 levels. Atomic Data Nucl. Data Tables 77 (1).
Cockayne, E., Shirley, E.L., Ravel, B., Woicik, J.C., 2018. Local atomic geometry and Ti 1s near-edge spectra in $PbTiO_3$ and $SrTiO_3$. Phys. Rev. B 98, 014111.
de Groot, F.M.F., Fuggle, J.C., Thole, B.T., Sawatzky, G.A., 1990. 2*p* x-ray absorption of 3*d* transition-metal compounds: an atomic multiplet description including the crystal field. Phys. Rev. B 41, 928.
Gilmore, K., Shirley, E.L., 2010. Numerical quantification of the vibronic broadening of the $SrTiO_3$ Ti L-edge spectrum. J. Phys. Condens. Matter 22, 315901.
Gilmore, K., Vinson, J., Shirley, E.L., Prendergast, D., Pemmaraju, C.D., Kas, J.J., Vila, F. D., Rehr, J.J., 2015. Efficient implementation of core-excitation Bethe-Salpeter equation calculations. Comput. Phys. Commun. 197, 109.
Lee, P.A., Pendry, J.B., 1975. Theory of the extended x-ray absorption fine structure. Phys. Rev. B 11, 2795.
Lee, P.A., Citrin, P.H., Eisenberger, P., Kincaid, B.M., 1981. Extended x-ray absorption fine structure—its strengths and limitations as a structural tool. Rev. Mod. Phys. 53, 769.
Pascal, T.A., Boesenberg, U., Kostecki, R., Richardson, T.J., Weng, T.C., Sokaras, D., Nordlund, D., McDermott, E., Moewes, A., Cabana, J., Prendergast, D., 2014. Finite temperature effects on the X-ray absorption spectra of lithium compounds: first-principles interpretation of X-ray Raman measurements. Phys. Rev. B 140, 034107.
Prendergast, D., Galli, G., 2006. X-ray absorption spectra of water from first principles calculations. Phys. Rev. Lett. 96, 215502.
Rehr, J.J., Albers, R.C., 2000. Theoretical approaches to x-ray absorption fine structure. Rev. Mod. Phys. 72, 621.
Shirley, E.L., Vinson, J., Gilmore, K., 2020. The OCEAN suite: core excitations. International Tables for Crystallography I. https://doi.org/10.1107/S157487072000333X, 2020.
Shirley, E.L., Woicik, J.C., 2022. Revisiting the K-edge X-ray absorption fine structure of Si, Ge-Si alloys, and the isoelectronic series: CuBr, ZnSe, GaAs, and Ge. Phys. Chem. Chem. Phys. 24, 20742.
Stern, E.A., 1974. Theory of the extended x-ray absorption fine structure. Phys. Rev. B 10, 3027.
Stern, E.A., Līviņš, P., Zhang, Z., 1991. Thermal vibration and melting from a local perspective. Phys. Rev. B 43, 8850.
Taillefumier, M., Cabaret, D., Flank, A., Mauri, F., 2002. X-ray absorption near-edge structure calculations with the pseudopotentials: application to the K edge in diamond and α-quartz. Phys. Rev. B 66, 195107.
Tinte, S., Shirley, E.L., 2008. Vibrational effects on $SrTiO_3$ Ti 1s absorption spectra studied using first-principles methods. J. Phys. Condens. Matter 20, 365221.
Vinson, J., Jach, T., Müller, M., Unterumsberger, R., Beckhoff, B., 2016. Quasiparticle lifetime broadening in resonant x-ray scattering of NH_4NO_3. Phys. Rev. B 94, 035163.
Woicik, J.C., List, R.S. List, Pate, B.B., Pianetta, P., 1988. Splitting of the "white line" 1s absorption edge in crystalline Si, SiGe, and dilute SiGe. Solid State Commun. 65, 685.
Woicik, J.C., Pianetta, P., 2015. Studies of Si-Ge interfaces with surface EXAFS and photoemission. In: Bachrach, R.Z. (Ed.), Synchrotron Radiation Research: Advances in Surface and Interface Science, vol. 2. Springer, Boston.
Woicik, J.C., Cockayne, E., Shirley, E.L., Levin, I., Weiland, C., Ravel, B., Abeykoon, A.M. M., 2023. Lattice vibrations and energy landscape of the isoelectronic semiconductor series CuBr, ZnSe, GaAs, and Ge: the special case of CuBr and its d-level chemistry. Phys. Rev. B 108, 195202.